Electronic Supplementary Material (ESI) for Polymer Chemistry.

Electronic Supplementary Information

Water-Based Polymer Colloids with a Branched Chain Architecture as Low-Gel Pressure-Sensitive Adhesives

Emily M. Brogden, Stefan A. F. Bon.*

The University of Warwick, Coventry CV4 7AL, UK.

Web: https://bonlab.info, *S.Bon@warwick.ac.uk

List of Figures

List of Tables

Table S1: Monomer compositions for each latex synthesized. The mole percentage quoted relates to the number of molecules and not the number of vinyl groups.

Sample	2-OA/ mol%	IBoMA/ mol%	AA/ mol%	EGDMA/ mol%	2-EHTG/ mol%
B_X04_C4	83.38	3.73	5.46	3.72	3.71
B_X07_C4	80.34	3.57	5.34	7.18	3.57
B_X16_C4	72.53	3.22	4.89	16.13	3.23
F_X00_C4	86.15	3.84	5.73	0	4.27
F_X08_C4	81.52	4.39	2.11	7.93	4.04
F_X11_C4	78.90	4.23	2.06	10.92	3.88
F_X13_C4	77.12	4.14	2.03	12.92	3.80
F_X18_C4	73.02	3.95	1.91	17.50	3.62
F_X00_C2	88.03	3.93	5.86	0	2.18
F_X08_C2	83.20	4.49	2.17	8.07	2.07
F_X11_C2	80.45	4.33	2.09	11.14	1.98
F_X13_C2	78.86	4.15	2.03	13.05	1.91
F_X18_C2	74.36	3.99	1.94	17.86	1.86
F_X13_C1	78.39	4.20	2.05	14.25	1.11
F_X13_C0.5	78.97	4.24	2.07	14.16	0.57

Table S2: Recipes for each latex synthesized.

Latex	Charge								Feed 1					Feed 2			
	2-OA / g	IBoMA / g	AA / g	EGDMA / g	2-EHTG / g	APS / g	H_2O / g	Lakeland PAE 136 / g	2-OA / g	IBoMA / g	AA / g	EGDMA / g	2-EHTG / g	Brij L23 / g	Lakeland PAE 136 / g	$NaHCO_3$ / g	H_2O / g
B_X04_C4	6.0697	0.3274	0.1555	0.2913	0.2996	0.1969	121.6246	0.3478	59.9031	3.1875	1.5136	2.8358	2.9169	2.0433	0.2443	0.5630	9.7165
B_X07_C4	5.8665	0.3144	0.1525	0.5637	0.2889	0.1965	121.8350	0.3515	57.7494	3.0953	1.5011	5.5487	2.8437	2.0258	0.2447	0.5575	9.6254
B_X16_C4	5.3319	0.2860	0.1406	1.2756	0.2632	0.1965	121.6950	0.3492	52.0877	2.7936	1.3735	12.4615	2.5716	2.0357	0.2459	0.5602	9.6721
F_X00_C4	6.2578	0.3365	0.1628	0	0.3443	0.1966	121.6449	0.3459	61.1951	3.2910	1.5922	0	3.3669	2.0453	0.2445	0.5631	9.7326
F_X08_C4	6.2854	0.3385	0.1627	0	0.3118	0.1969	121.6546	0.3466	54.3508	2.9313	1.5662	5.8843	3.0002	1.9968	0.2393	0.5508	9.5297
F_X11_C4	6.2872	0.3374	0.1645	0	0.3092	0.1966	121.6249	0.3481	53.7040	2.8876	1.5711	8.3122	2.9528	2.0430	0.2447	0.5630	9.7089
F_X13_C4	6.2861	0.3373	0.1653	0	0.3098	0.1966	121.6449	0.3485	52.2114	2.8082	1.5393	9.8058	2.8855	2.0407	0.2444	0.5624	9.6981
F_X18_C4	6.2831	0.3395	0.1647	0	0.3115	0.1969	121.9146	0.3478	49.2538	2.6706	1.4592	13.3408	2.7593	2.0277	0.2430	0.5593	9.6774
F_X00_C2	6.3993	0.3448	0.1667	0	0.1966	121.8449	0.3471	0.3471	61.7542	3.3271	1.6085	0	1.6931	2.0581	0.2460	0.5666	9.7938
F_X08_C2	6.4124	0.3458	0.1669	0	0.1597	0.1930	121.8385	0.3463	56.5808	3.0557	1.6428	6.1248	1.5718	2.0392	0.2470	0.5613	9.6983
F_X11_C2	6.4146	0.3448	0.1669	0	0.1582	0.1962	121.7453	0.3512	54.8600	2.9553	1.5964	8.4964	1.5125	2.0374	0.2447	0.5622	9.6901
F_X13_C2	6.4241	0.3382	0.1650	0	0.1560	0.1962	121.6953	0.3468	53.3074	2.8135	1.5330	9.8773	1.4492	2.0037	0.2406	0.5529	9.5300
F_X18_C2	6.4131	0.3439	0.1675	0	0.1602	0.1930	121.5685	0.3488	49.3668	2.6573	1.4613	13.4350	1.3972	1.9966	0.2419	0.5496	9.4958
F_X13_C1	6.4709	0.3464	0.1692	0	0.0920	0.1965	121.6750	0.3490	52.9906	2.8448	1.5566	10.8235	0.8460	2.0415	0.2442	0.5620	9.7056
F_X13_C0.5	6.5081	0.3491	0.1704	0	0.0470	0.1965	121.6850	0.3483	53.4100	2.8726	1.5708	10.7551	0.4334	2.0097	0.2404	0.5533	9.5544

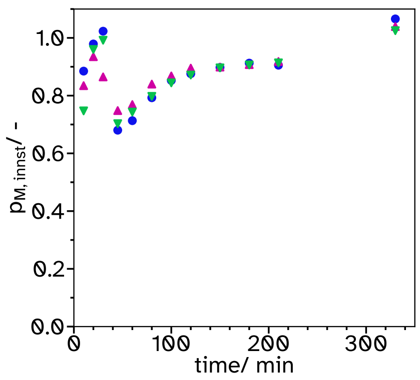

(a) Instantaneous monomer conversion, $\rho_{M,inst}$, over time.

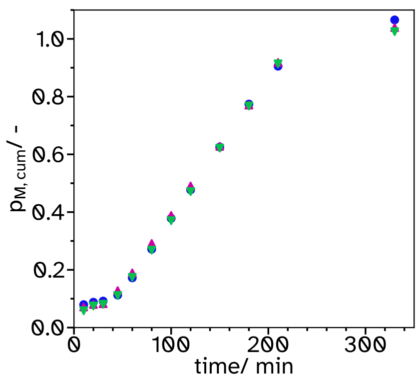

(b) Cumulative monomer conversion, $\rho_{M,cum}$, over time.

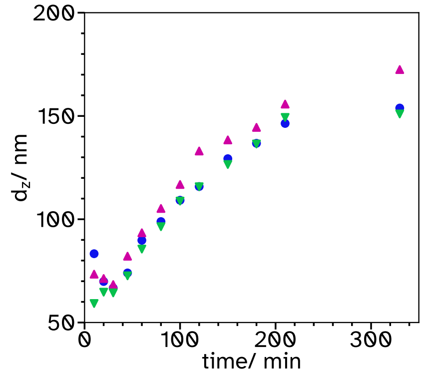

(c) Average hydrodynamic diameter, d_z, over time.

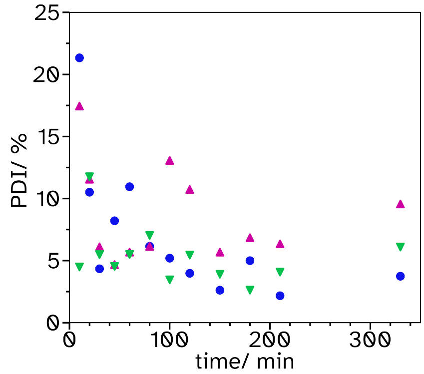

(d) Average particle dispersity index, *PDI*, over time.

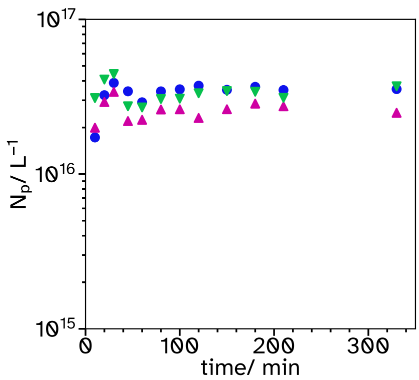

(e) Average number of particles, N_p, over time.

Figure S1: Kinetics and particle size evolution for B_Xn_C4 where n= 4 ●, 7 ▲ and 16 ▼.

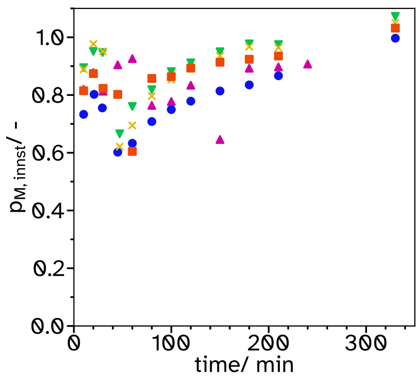

(a) Instantaneous monomer conversion, $\rho_{M,inst}$, over time.

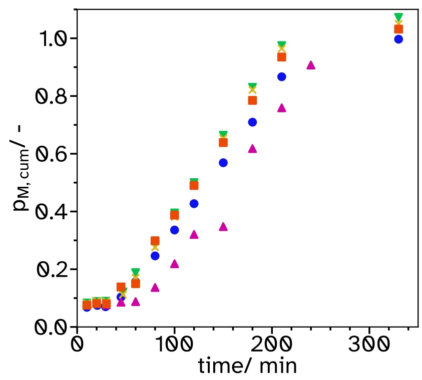

(b) Cumulative monomer conversion, $\rho_{M,cum}$, over time.

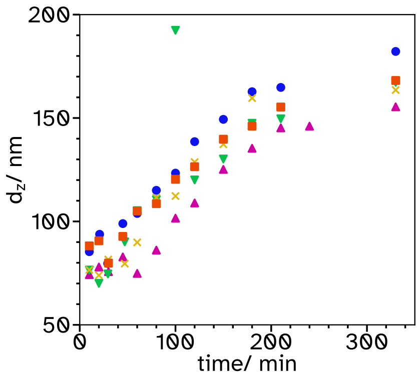

(c) Average hydrodynamic diameter, d_z, over time.

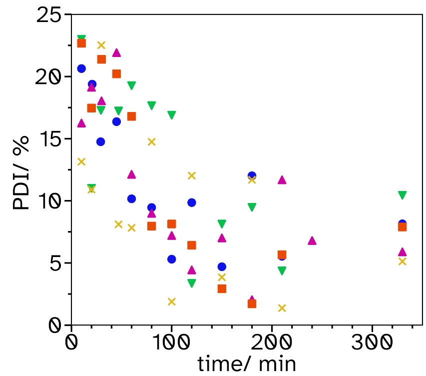

(d) Average particle dispersity index, *PDI*, over time.

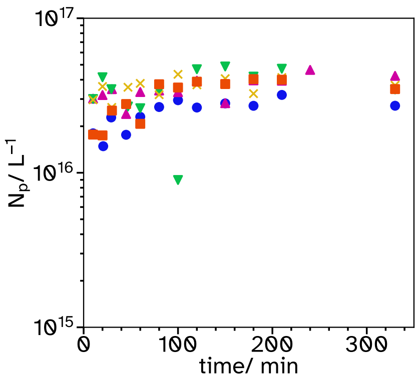

(e) Average number of particles, N_p, over time.

Figure S2: Kinetics and particle size evolution for F_Xn_C4 where n= 0 ●, 8 ▲, 11 ▼, 13 × and 18 ■.

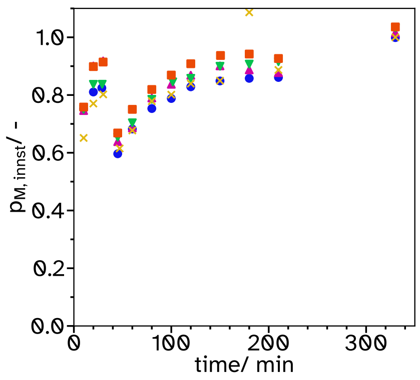

(a) Instantaneous monomer conversion, $\rho_{M,inst}$, over time.

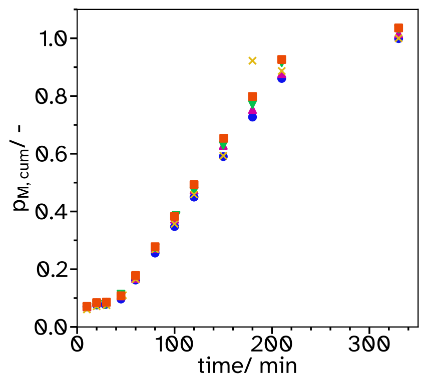

(b) Cumulative monomer conversion, $\rho_{M,cum}$, over time.

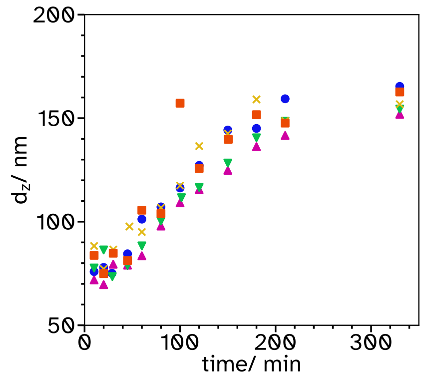

(c) Average hydrodynamic diameter, d_z, over time.

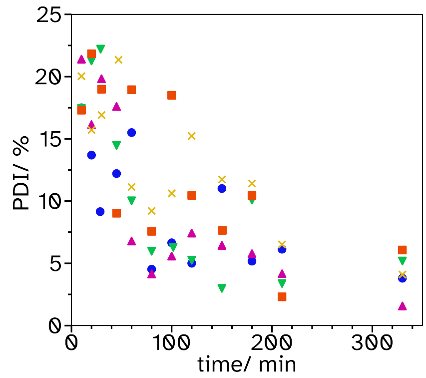

(d) Average particle dispersity index, *PDI*, over time.

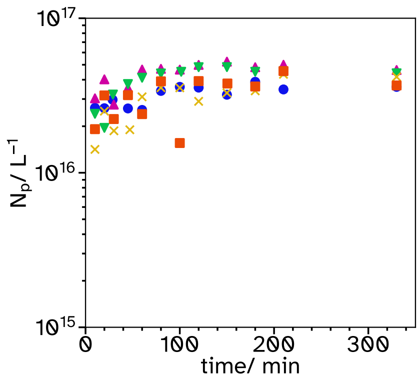

(e) Average number of particles, N_p, over time.

Figure S3: Kinetics and particle size evolution for F_Xn_C2 where n= 0 ●, 8 ▲, 11 ▼, 13 × and 18 ■.

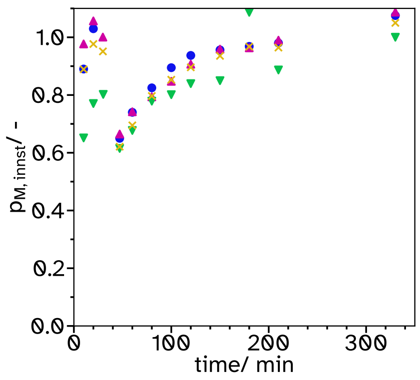

(a) Instantaneous monomer conversion, $\rho_{M,inst}$, over time.

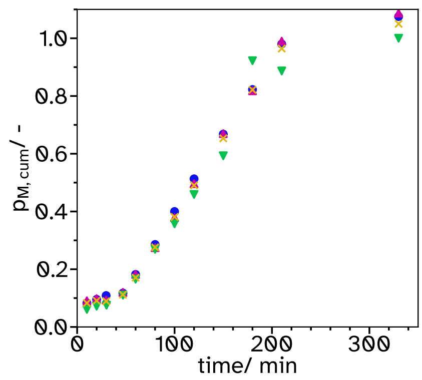

(b) Cumulative monomer conversion, $\rho_{M,cum}$, over time.

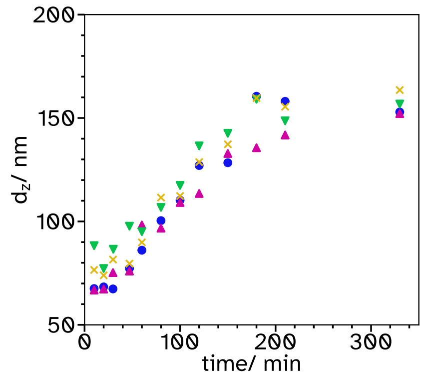

(c) Average hydrodynamic diameter, d_z, over time.

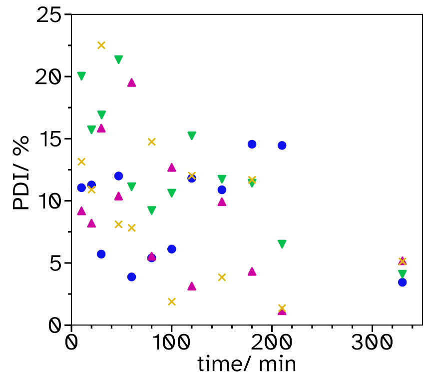

(d) Average particle dispersity index, *PDI*, over time.

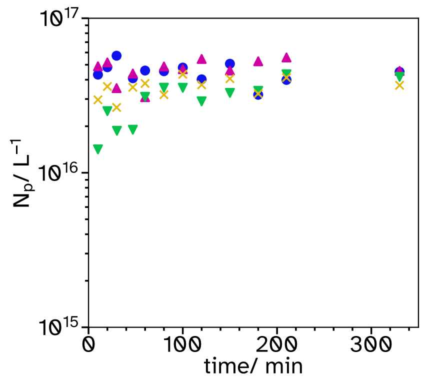

(e) Average number of particles, N_p, over time.

Figure S4: Kinetics and particle size evolution for F_X13_Cn where n= 0.5 ●, 1 ▲, 2 ▼, and 4 ×.

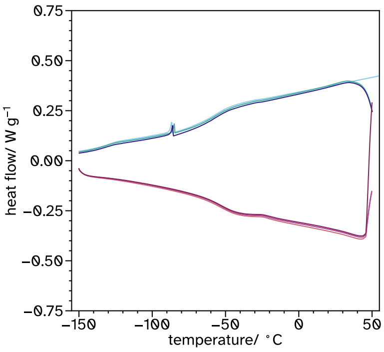

(a) n= 4

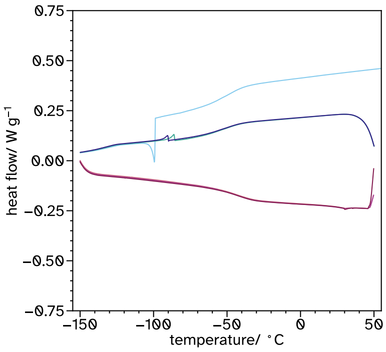

(b) n= 7

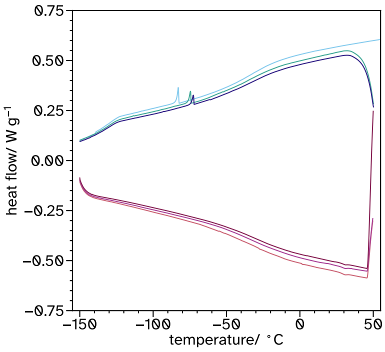

(c) n= 16

Figure S5: DSC thermograms for B_Xn_C4.

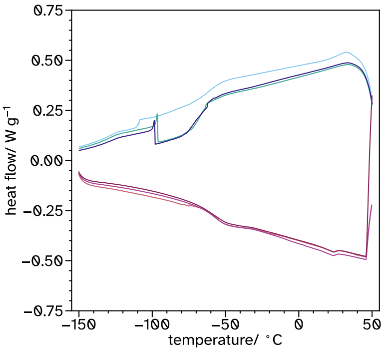

(a) n= 0

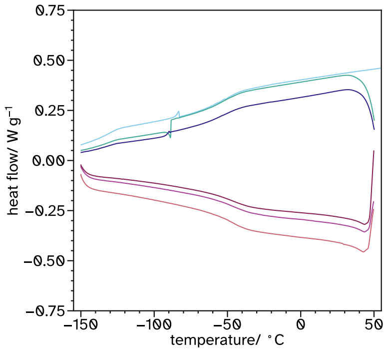

(b) n= 8

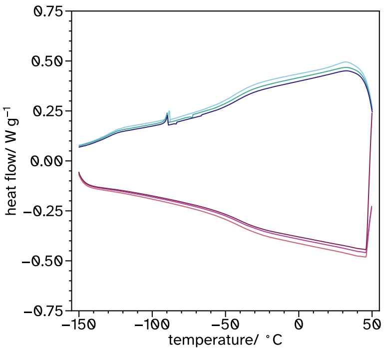

(c) n= 11

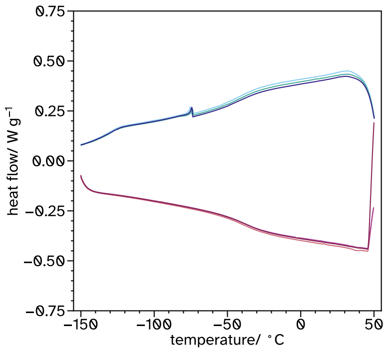

(d) n= 13

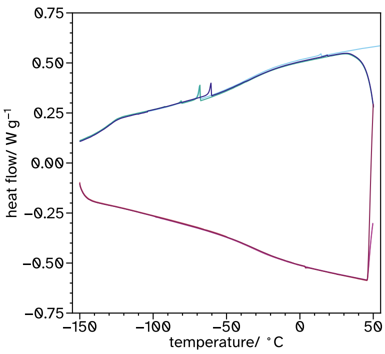

(e) n= 18

Figure S6: DSC thermograms for F_Xn_C4.

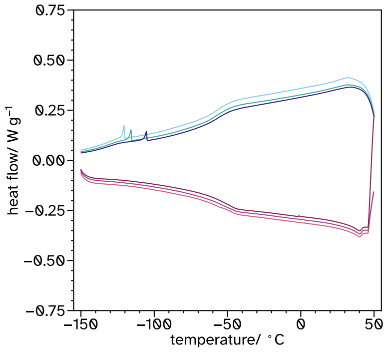

(a) n= 0

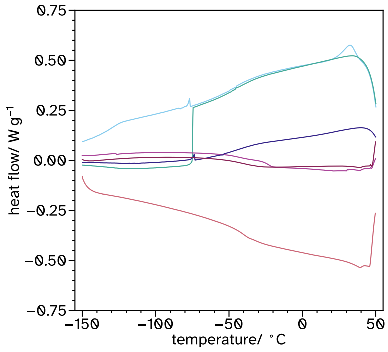

(b) n= 8

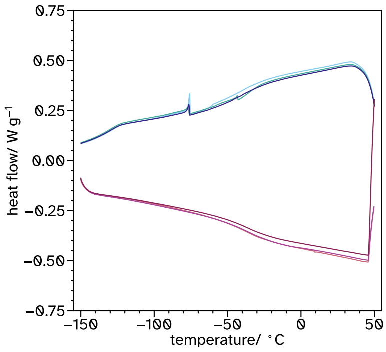

(c) n= 11

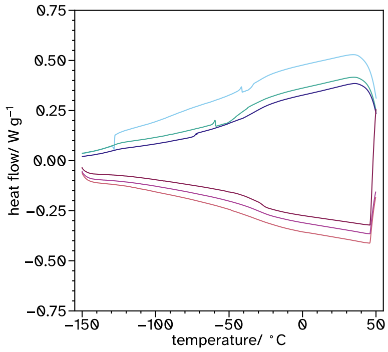

(d) n= 13

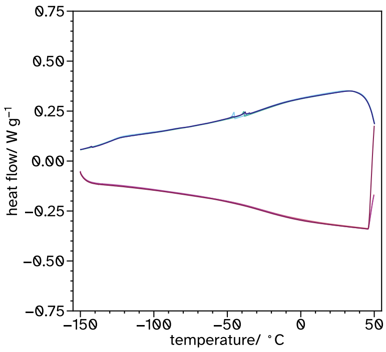

(e) n= 18

Figure S7: DSC thermograms for F_Xn_C2.

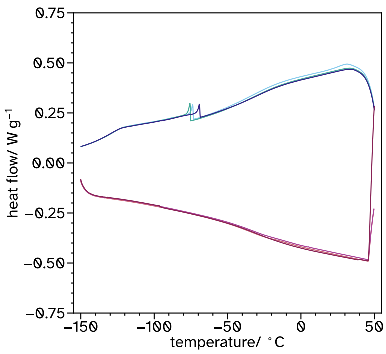

(a) n= 1

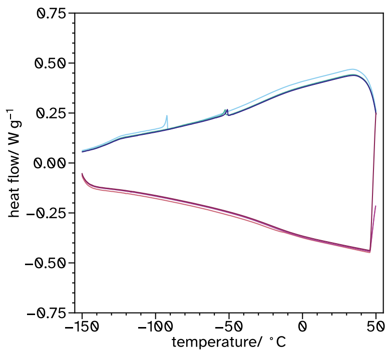

(b) n= 0.5

Figure S8: DSC thermograms for F_X13_Cn.

Table S3: Glass transition temperature, T_g, analyses for all latexes synthesized.

Latex	Cooling Midpoint/ °C			Cooling Onset/ °C			Heating Midpoint/ °C			Heating Onset/ °C		
	1	2	3	1	2	3	1	2	3	1	2	3
B_X04_C4	-61.28	-59.13	-60.28	-49.48	-48.23	-49.69	-56.84	-58.26	**-58.45**	-64.11	-64.37	-66.38
B_X07_C4	-49.07	-56.29	-51.41	-38.65	-38.75	-39.78	-41.30	-44.01	**-42.74**	-56.26	-61.30	-58.46
B_X16_C4	-35.97	-37.09	-38.36	-9.89	-16.24	-13.58	-28.38	-33.27	**-30.72**	-58.30	-53.65	-49.29
F_X00_C4	-61.91	-68.44	-67.18	-52.15	-62.60	-60.40	-55.72	-56.85	**-56.72**	-62.49	-66.23	-69.37
F_X08_C4	-59.70	-42.99	-59.57	-40.11	-40.10	-40.29	-44.88	-44.88	**-46.02**	-57.25	-58.46	-57.28
F_X11_C4	-46.61	-46.85	-44.91	-26.29	-24.34	-27.45	-40.75	-42.28	**-42.53**	-57.18	-58.75	-55.36
F_X13_C4	-42.76	-43.30	-42.46	-22.71	-20.55	-21.88	-44.77	-37.67	**-37.88**	-61.44	-52.61	-53.09
F_X18_C4	-36.62	-39.97	-41.59	-14.32	-16.61	-14.55	-34.29	-28.64	**-33.05**	-52.59	-45.66	50.34
F_X00_C2	-60.10	-59.57	-60.40	-46.04	-44.77	-47.84	-55.68	-53.93	**-54.67**	-62.99	-62.52	-64.20
F_X08_C2	-49.38	-	-47.98	-29.25	-	-29.63	-40.99	-32.30	**-42.81**	-49.90	-55.46	-54.42
F_X11_C2	-41.90	-31.93	-39.46	-27.18	-23.99	-31.82	-36.44	-34.75	**-38.67**	-52.69	-52.91	-54.72
F_X13_C2	-31.59	-39.49	-35.90	-27.33	-28.45	-24.91	-35.22	-30.14	**-29.41**	-53.37	-44.42	-35.41
F_X18_C2	-29.46	-24.67	-18.67	-6.96	-7.28	-1.47	-25.44	-25.89	**-26.80**	-46.61	-49.12	-48.60
F_X13_C1	-38.11	-36.28	-36.46	-13.46	-11.62	-14.44	-37.37	-37.47	**-31.73**	-53.68	-56.60	-52.38
F_X13_C0.5	-41.90	-26.43	-26.47	-6.72	-3.99	-6.80	-30.03	-22.63	**-25.14**	-48.45	-43.39	-45.67

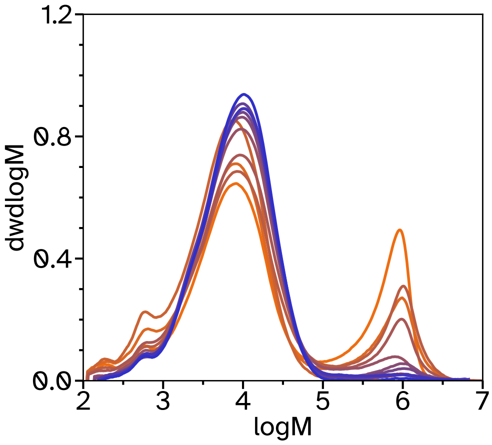

(a) n = 7

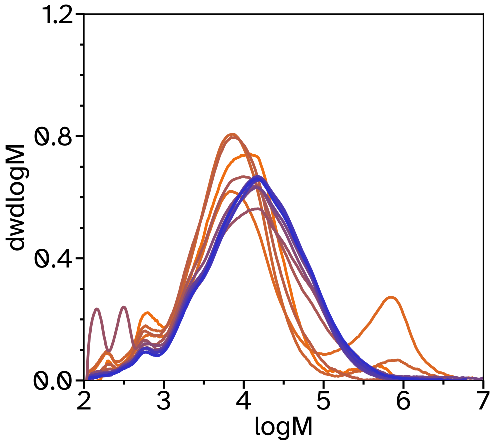

(b) n = 16

Figure S9: The molecular weight distributions from conventional SEC analysis for B_Xn_C4 from 10 *min* ■ to the final sample at 330 *min* ■.

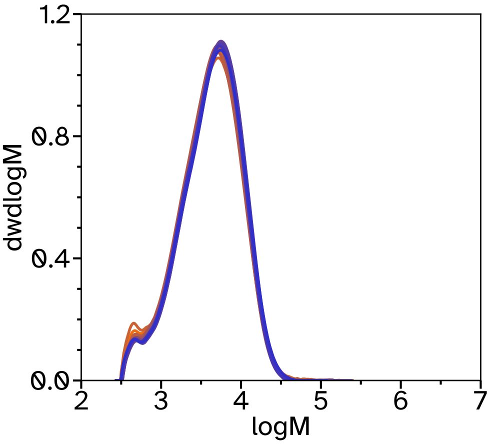

(a) n = 0

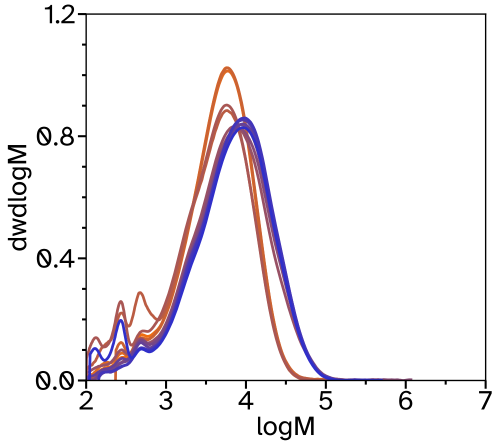

(b) n = 8

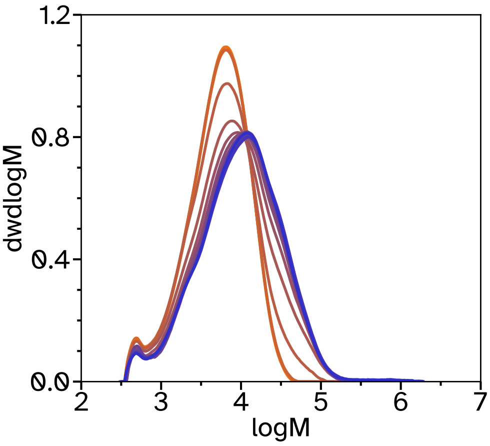

(c) n = 11

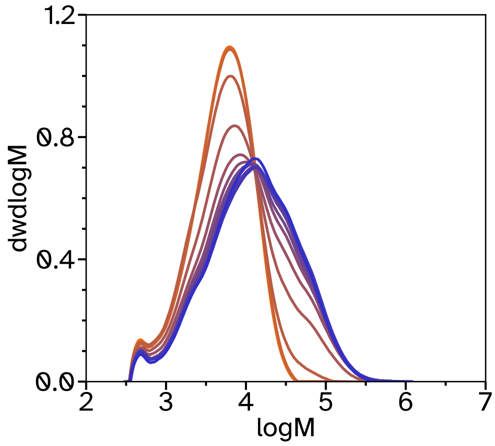

(d) n = 13

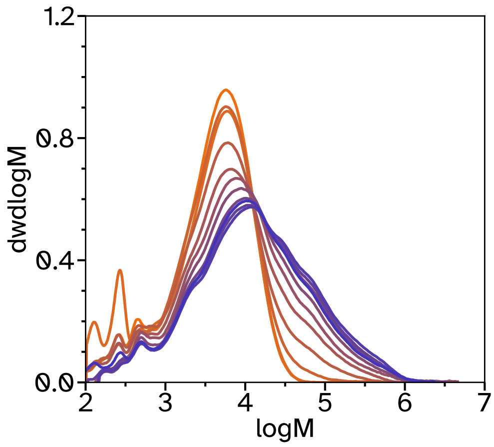

(e) n = 18

Figure S10: The molecular weight distributions from conventional SEC analysis for F_Xn_C4 from 10 *min* ■ to the final sample at 330 *min* ■.

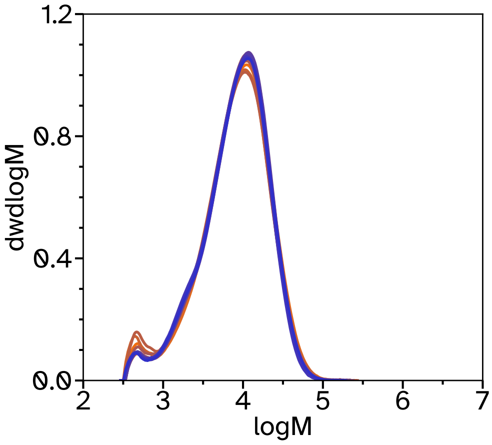

(a) n = 0

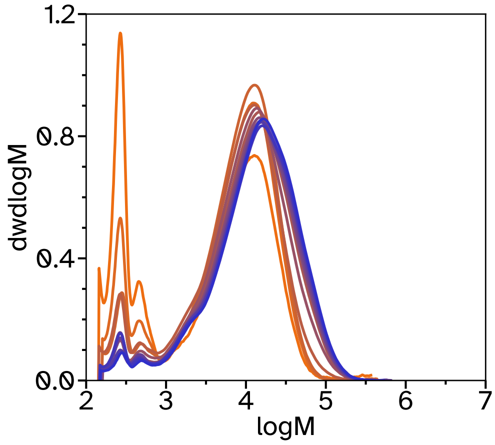

(b) n = 8

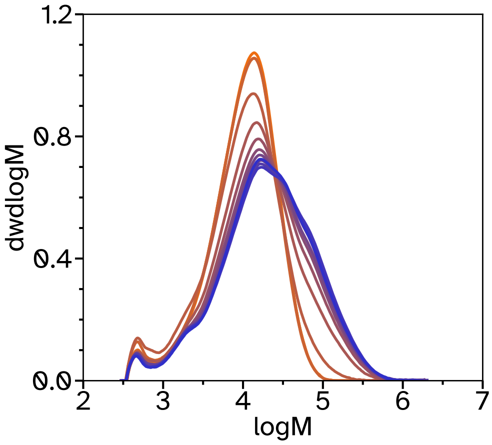

(c) n = 11

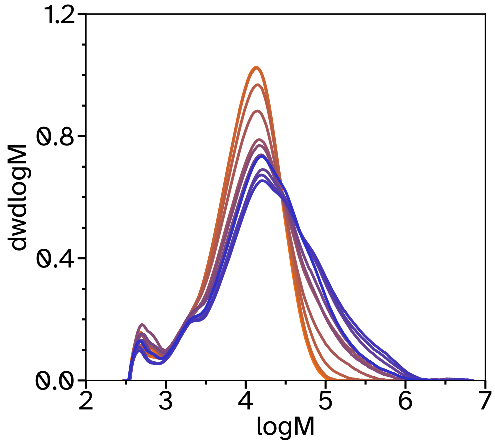

(d) n = 13

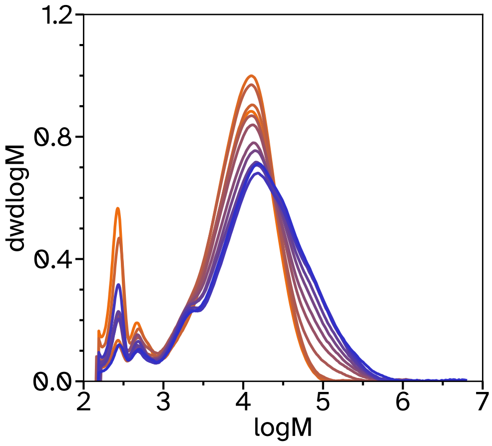

(e) n = 18

Figure S11: The molecular weight distributions from conventional SEC analysis for F_Xn_C2 from 10 *min* ■ to the final sample at 330 *min* ■.

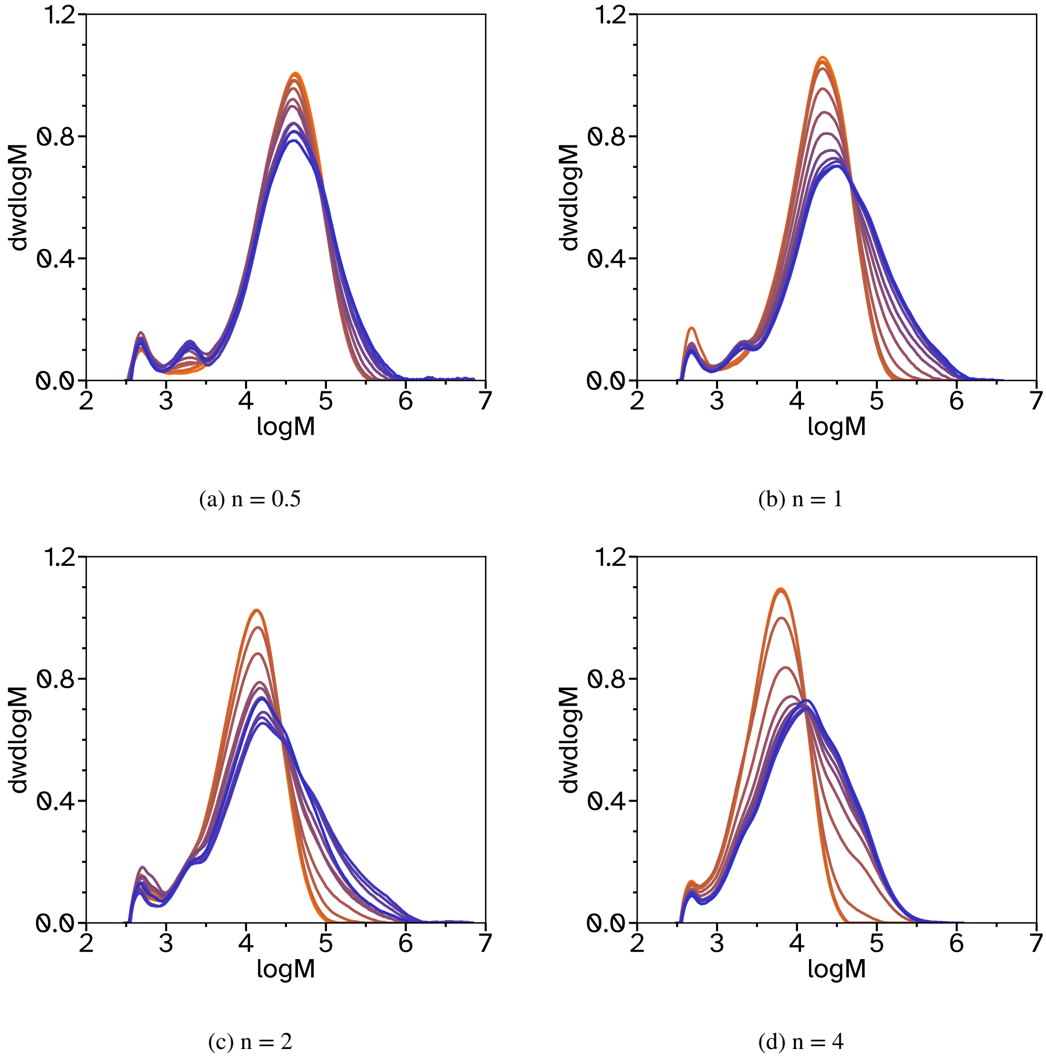

(a) n = 0.5

(b) n = 1

(c) n = 2

(d) n = 4

Figure S12: The molecular weight distributions from conventional SEC analysis for F_X13_Cn from 10 *min* ■ to the final sample at 330 *min* ■.

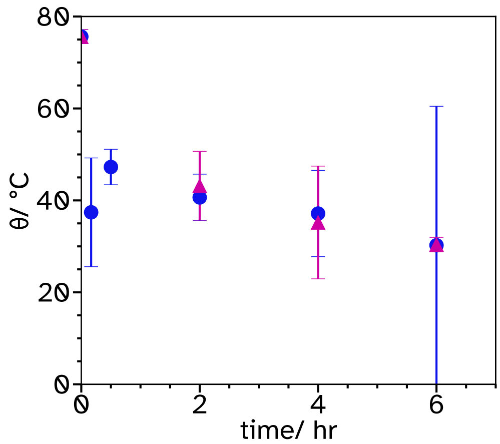

Figure S13: The contact angles of water droplets on the PET substrate after chemical modification for various times at 30 (●) and 60 (▲) °C. The contact angle with no modification is shown at 0 *h*.

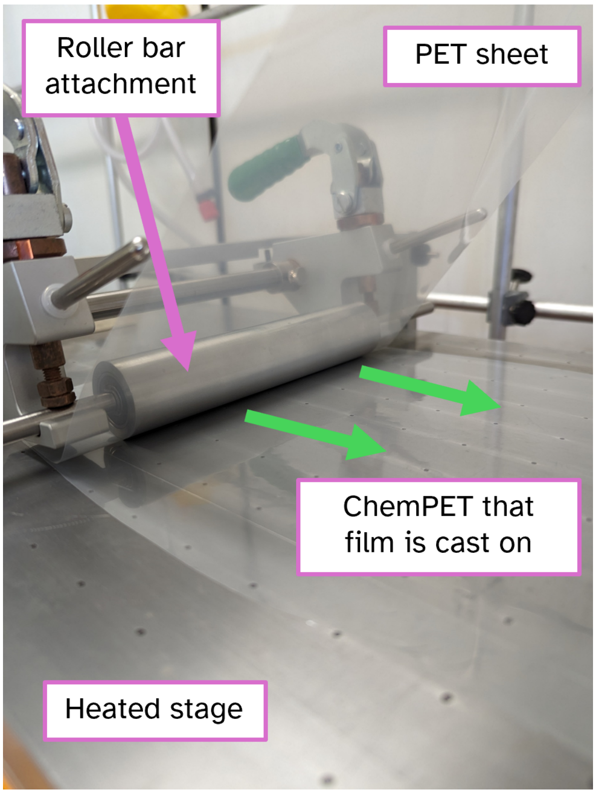

Figure S14: Cylindrical roller bar attachment on an Elcometer 4340 Automatic Film Applicator, which enabled a second sheet of PET to be adhered to the cast films with minimal bubbles. The green arrows show the direction of movement.

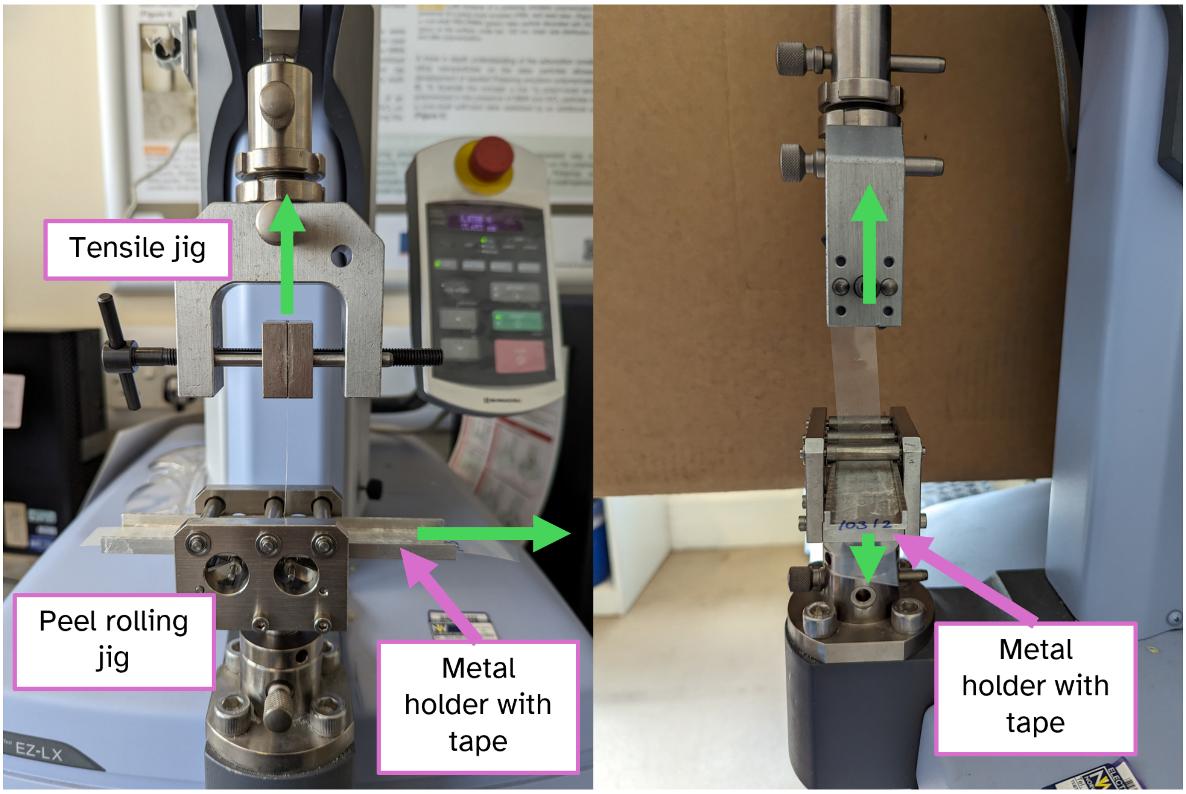

Figure S15: A Shimadzu EZ-LX universal testing machine with a 500 N tensile jig in the upper position and a peel rolling jig in the lower position which can hold a custom-made metal holder used for peel adhesion tests. The green arrows show the direction of movement.

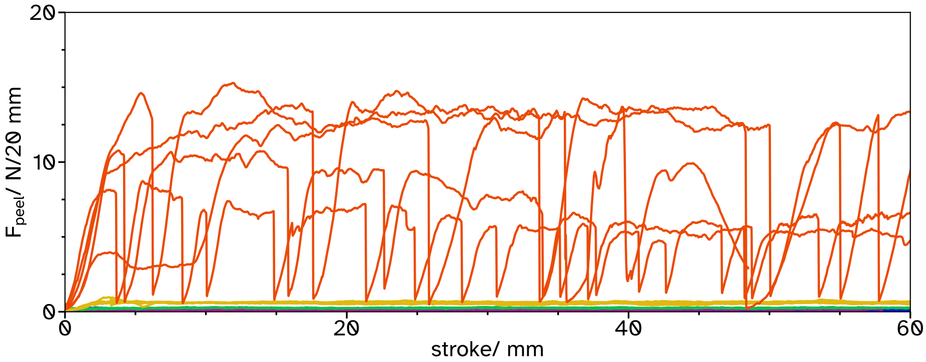

(a) All raw data shown.

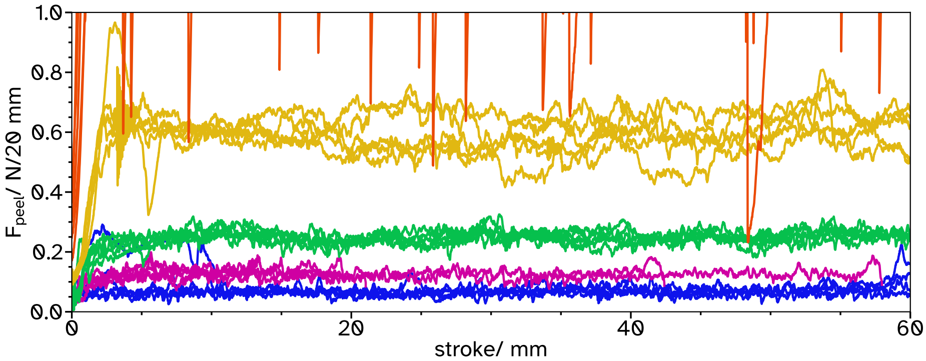

(b) Zoom in on raw data with low F_{peel}.

Figure S16: Peel adhesion force, F_{peel} as a function of peel distance, stroke for F_Xn_C4 where n = 0 ■, 8 ■, 11 ■, 13 ■ and 18 ■.

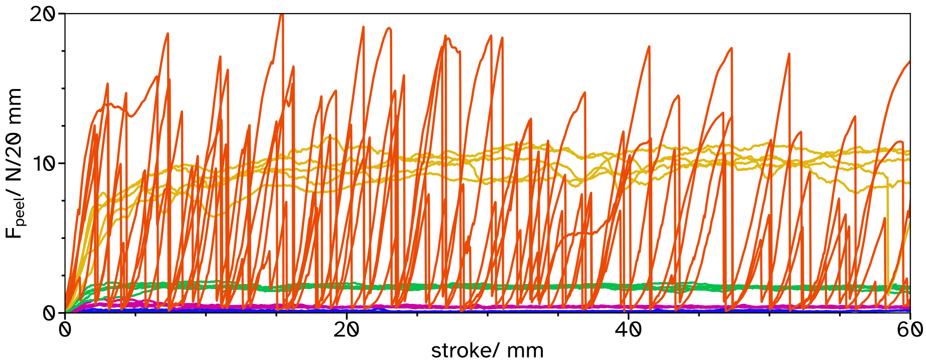

Figure S17: Peel adhesion force, F_{peel} as a function of peel distance, stroke for F_Xn_C2 where n = 0 ■, 8 ■, 11 ■, 13 ■ and 18 ■.

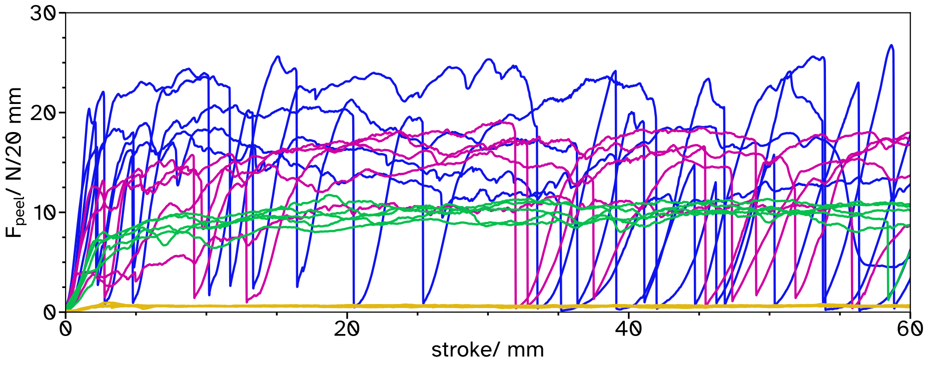

Figure S18: Peel adhesion force, F_{peel} as a function of peel distance, stroke for F_X13_Cn where n= 0.5 ■, 1 ■, 2 ■ and 4 ■.

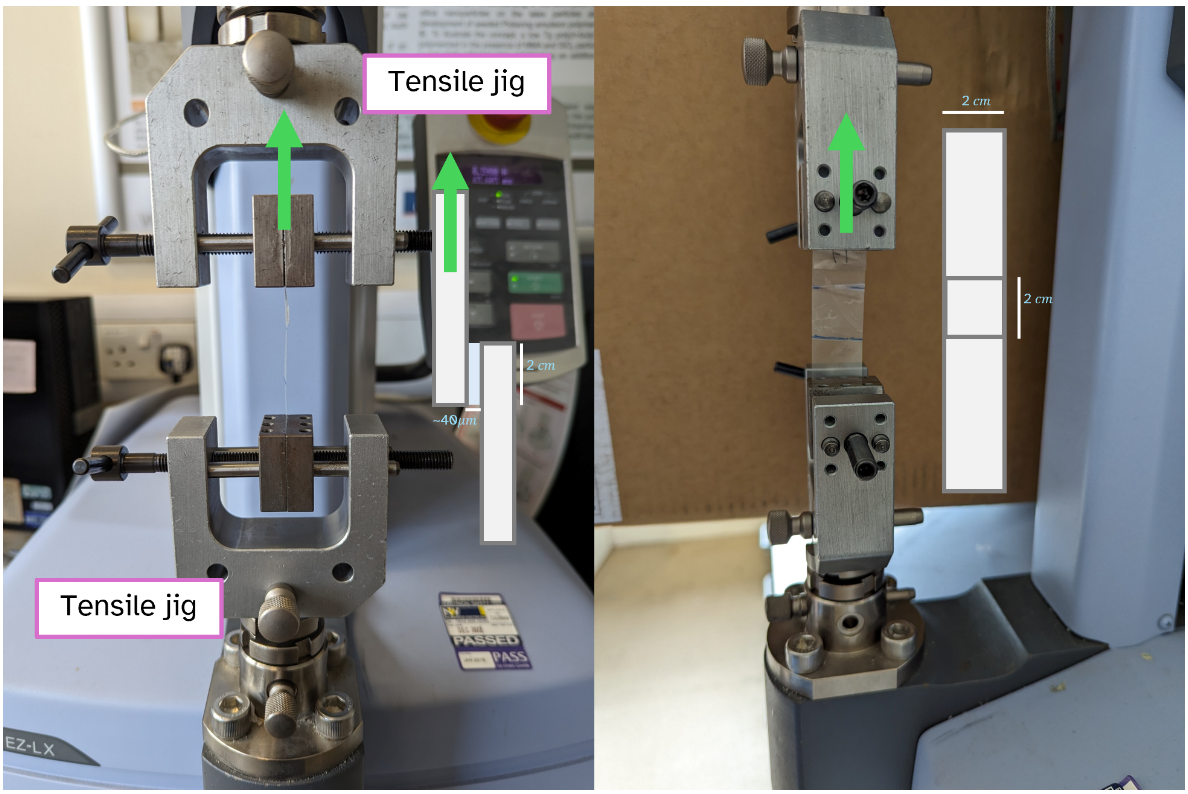

Figure S19: A Shimadzu EZ-LX universal testing machine with 500 N tensile jigs in the upper and lower positions, which held strips of tape connected by a lap joint for shear strength tests.Diagrams are shown within the images to demonstrate the lap joint where the PET is represented the grey outlined shapes and the adhesive is light blue. The green arrows show the direction of movement.

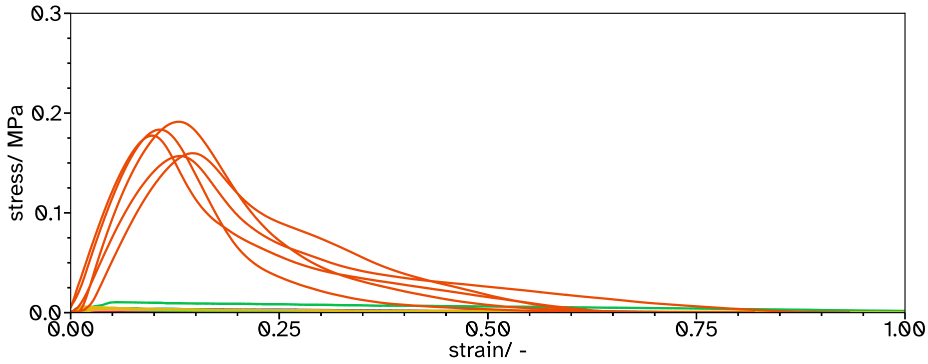

Figure S20: Stress-strain curves to obtain shear strength, W_{shear}, as the area under the curves for F_Xn_C4 where n = 0 ■, 8 ■, 11 ■, 13 ■ and 18 ■.

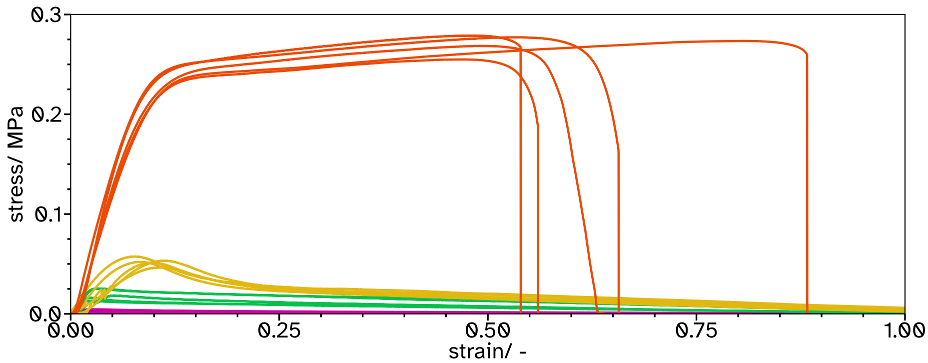

Figure S21: Stress-strain curves to obtain shear strength, W_{shear}, as the area under the curves for F_Xn_C2 where n = 0 ■, 8 ■, 11 ■, 13 ■ and 18 ■.

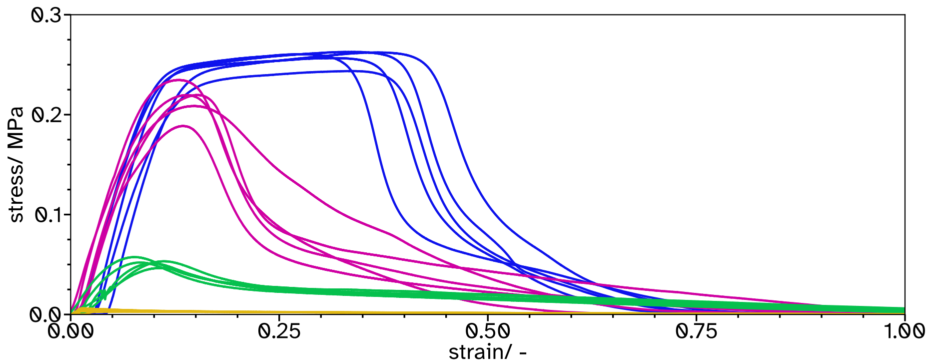

Figure S22: Stress-strain curves to obtain shear strength, W_{shear}, as the area under the curves for F_X13_Cn where n= 0.5 ■, 1 ■, 2 ■ and 4 ■.

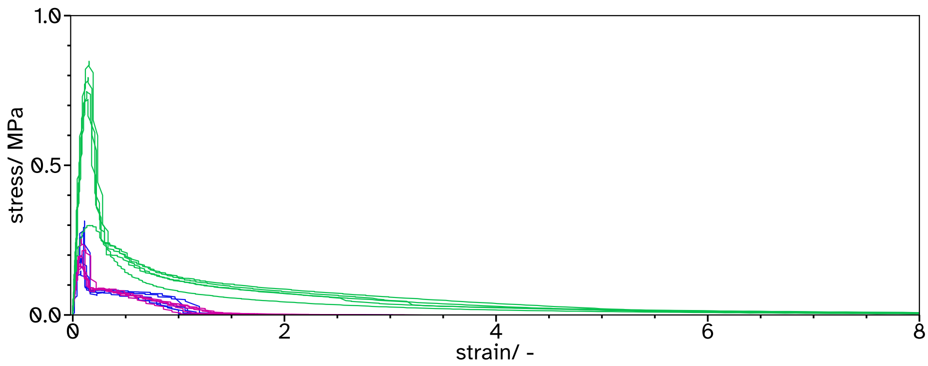

Figure S23: Stress-strain curves to obtain tack adhesion energy, W_{adh}, as the area under the curves for B_Xn_C4 where n = 4■, 7 ■, 16 ■.

Table S4: Average film heights during tack testing (average of 5 repeats) and rheological amplitude and frequency sweeps (average during the measurement).

Latex	Film height (W_{adh})/ μm	Film height (amp sweep)/ μm	Film height (freq sweep)/ μm
B_X04_C4	301 ± 29	203.49 ± 0.06	138.30 ± 0.02
B_X07_C4	414 ± 27	213.71 ± 0.06	220.63 ± 0.02
B_X16_C4	716 ± 163	646.07 ± 0.04	675.39 ± 0.02
F_X00_C4	153 ± 28	79.43 ± 0.05	239.55 ± 0.04
F_X08_C4	222 ± 63	193.46 ± 0.04	340.48 ± 0.02
F_X11_C4	391 ± 20	427.46 ± 0.04	359.48 ± 0.02
F_X13_C4	527 ± 37	475.79 ± 0.06	610.29 ± 0.07
F_X18_C4	642 ± 61	112.74 ± 0.05	353.71 ± 0.02
F_X00_C2	285 ± 38	127.95 ± 0.05	154.86 ± 0.02
F_X08_C2	432 ± 37	349.79 ± 0.06	382.94 ± 0.02
F_X11_C2	616 ± 11	553.74 ± 0.05	833.77 ± 0.03
F_X13_C2	722 ± 134	736.07 ± 0.05	672.03 ± 0.02
F_X18_C2	762 ± 75	684.79 ± 0.05	521.38 ± 0.02
F_X13_C1	940 ± 62	844.93 ± 0.04	643.97 ± 0.02
F_X13_C0.5	976 ± 22	829.69 ± 0.06	792.25 ± 0.02

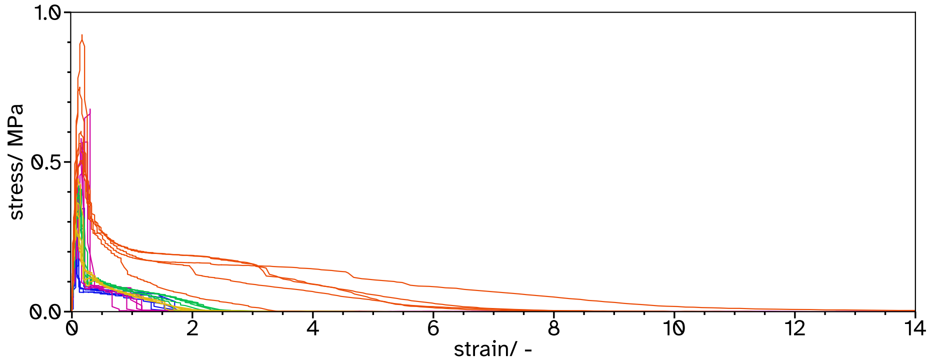

Figure S24: Stress-strain curves to obtain tack adhesion energy, W_{adh}, as the area under the curves for F_Xn_C4 where n = 0 ■, 8 ■, 11 ■, 13 ■ and 18 ■.

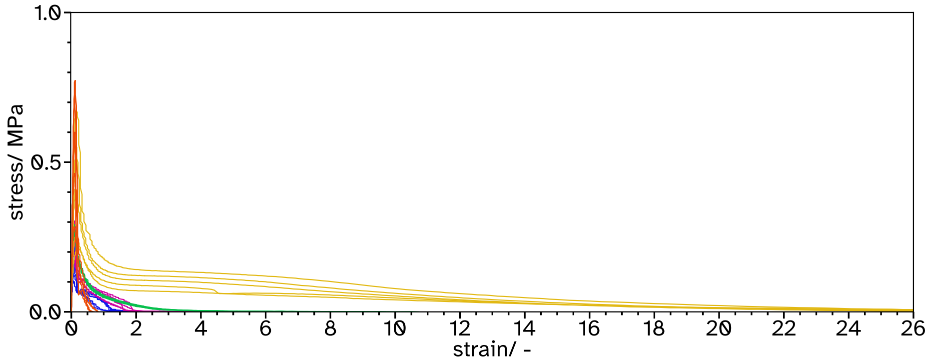

Figure S25: Stress-strain curves to obtain tack adhesion energy, W_{adh}, as the area under the curves for F_Xn_C2 where n = 0 ■, 8 ■, 11 ■, 13 ■ and 18 ■.

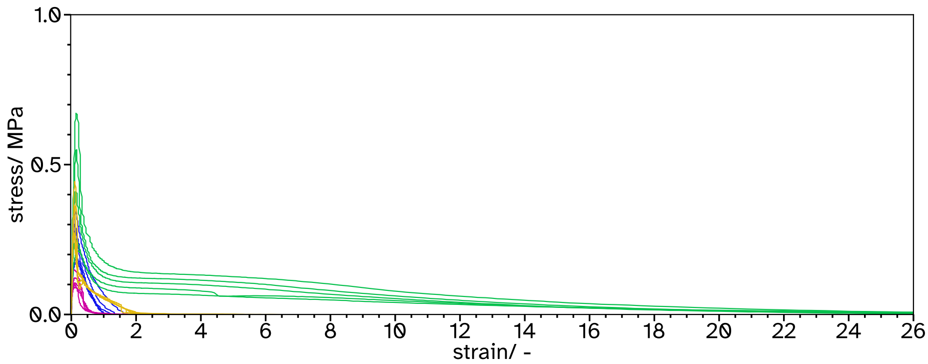

Figure S26: Stress-strain curves to obtain tack adhesion energy, W_{adh}, as the area under the curves for F_X13_Cn where n= 0.5 ■, 1 ■, 2 ■ and 4 ■.

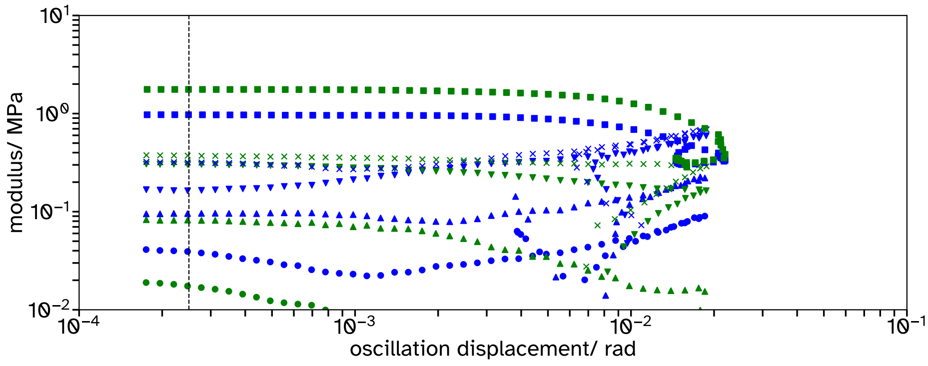

Figure S27: Amplitude sweeps with the storage modulus, G' ■, and loss modulus, G'' ■, for F_Xn_C4 where n= 0 ●, 8 ▲, 11 ▼, 13 × and 18 ■. The verticle black line shows the displacement used in the frequency sweeps to remain in the linear viscoelastic regime.

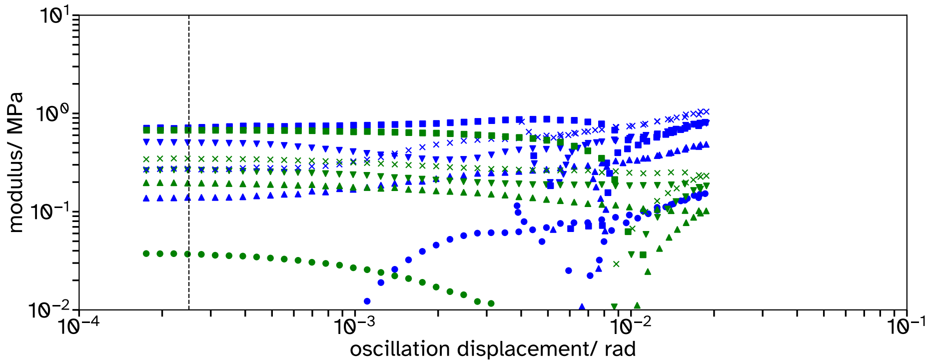

Figure S28: Amplitude sweeps with the storage modulus, G' ■, and loss modulus, G'' ■, for F_Xn_C2 where n= 0 ●, 8 ▲, 11 ▼, 13 × and 18 ■. The verticle black line shows the displacement used in the frequency sweeps to remain in the linear viscoelastic regime.

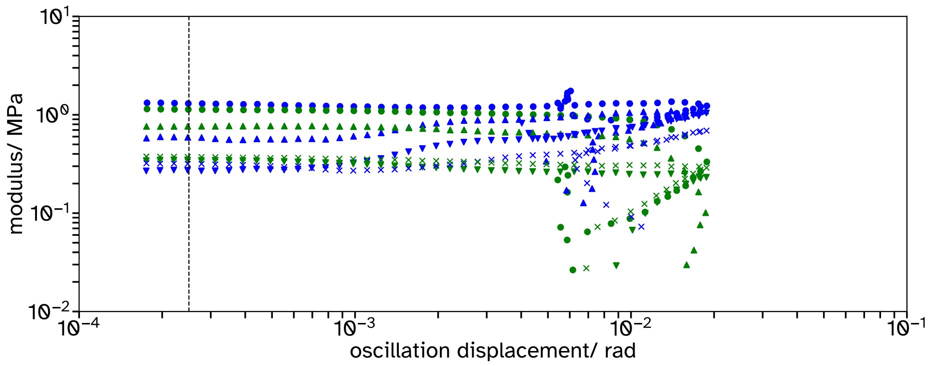

Figure S29: Amplitude sweeps with the storage modulus, G' ■, and loss modulus, G'' ■, for F_X13_Cn where n= 0.5 ●, 1 ▲, 2 ▼, and 4 ×. The verticle black line shows the displacement used in the frequency sweeps to remain in the linear viscoelastic regime.

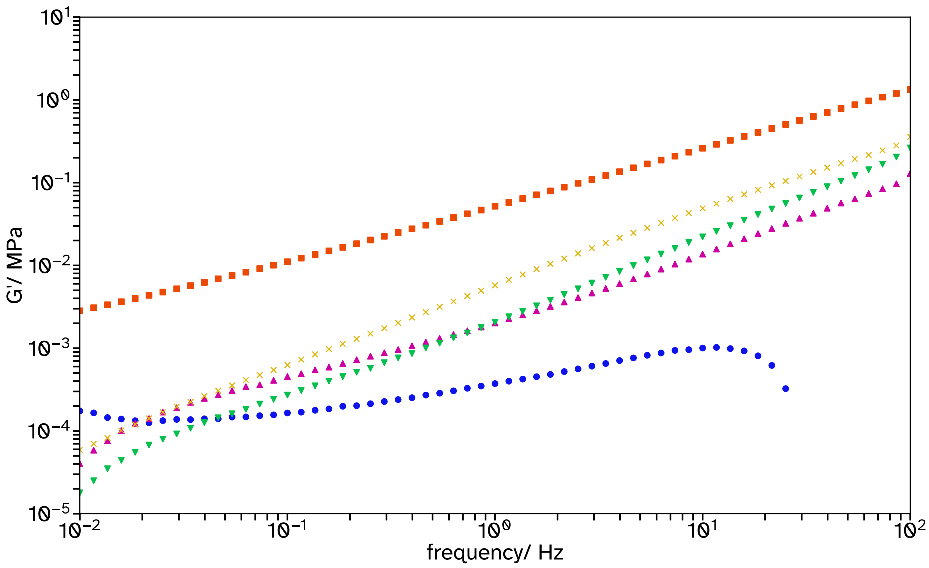

(a)

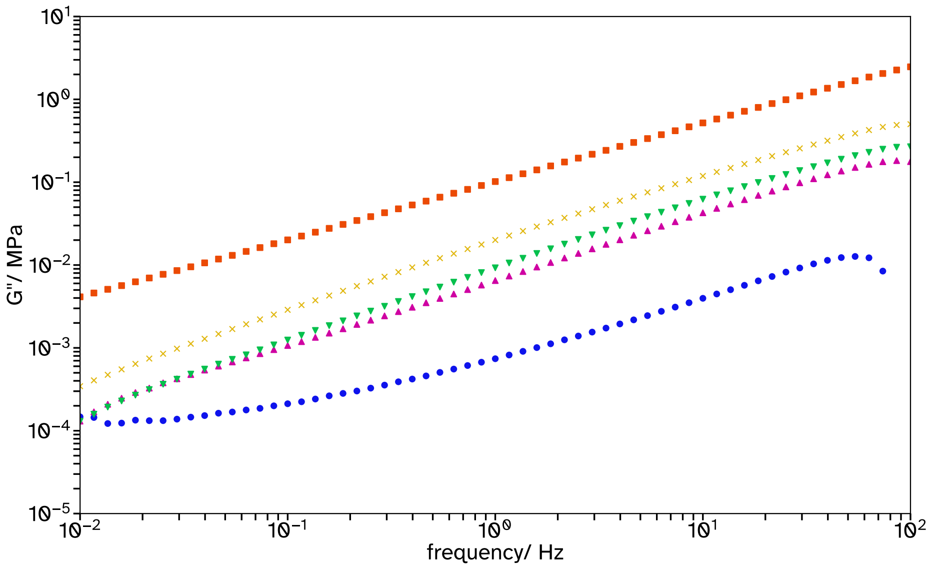

(b)

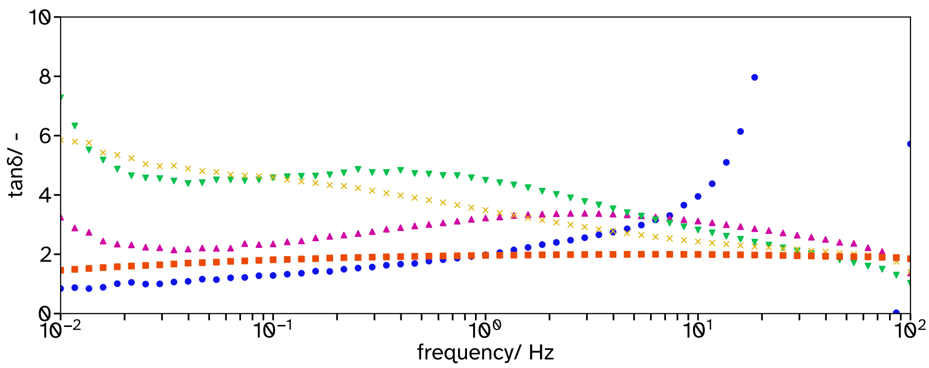

(c)

Figure S30: Rheological frequency sweeps of F_Xn_C4 where n= 0 ●, 8 ▲, 11 ▼, 13 × and 18 ■.

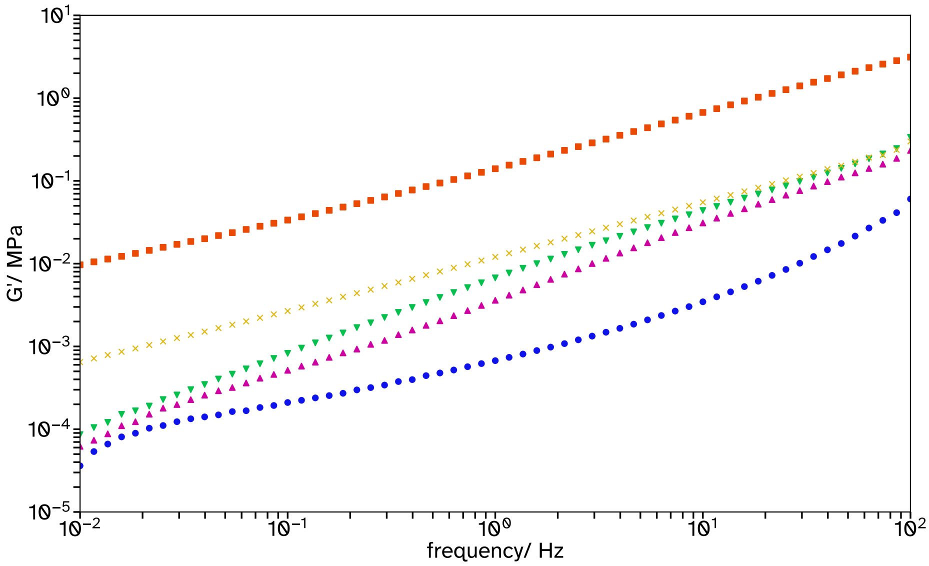

(a)

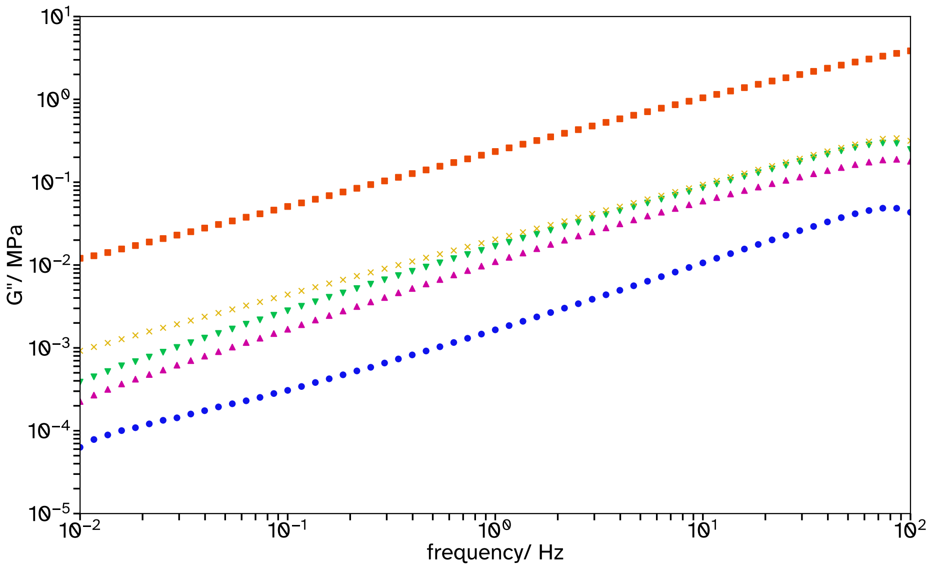

(b)

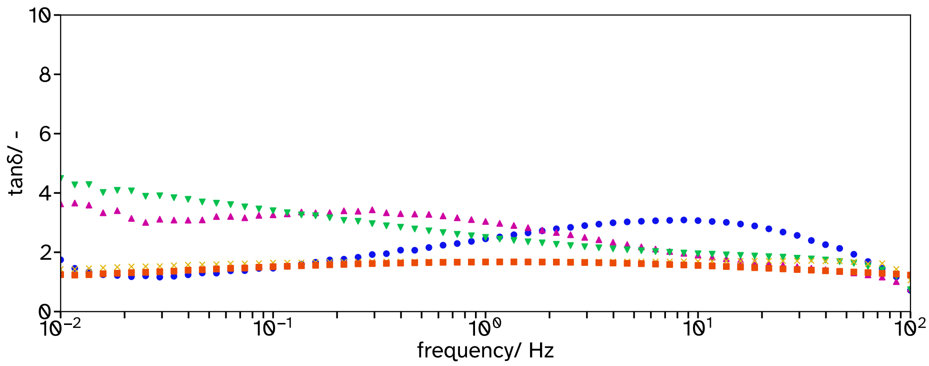

(c)

Figure S31: Rheological frequency sweeps of F_Xn_C2 where n= 0 ●, 8 ▲, 11 ▼, 13 × and 18 ■.

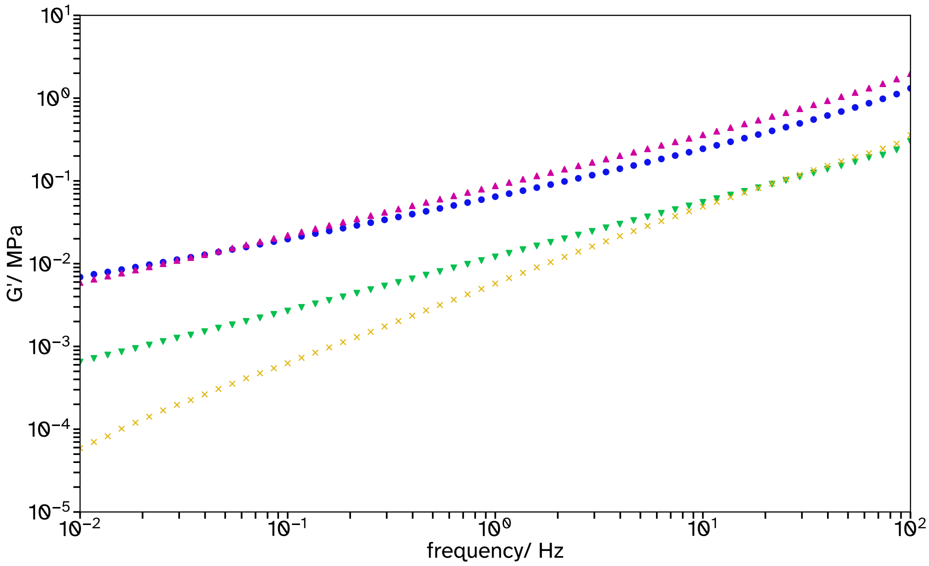

(a)

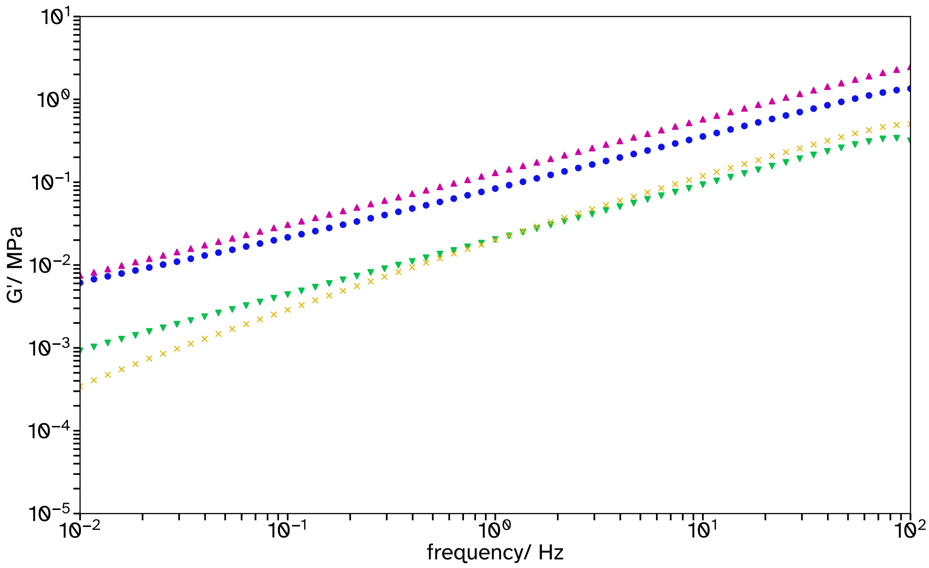

(b)

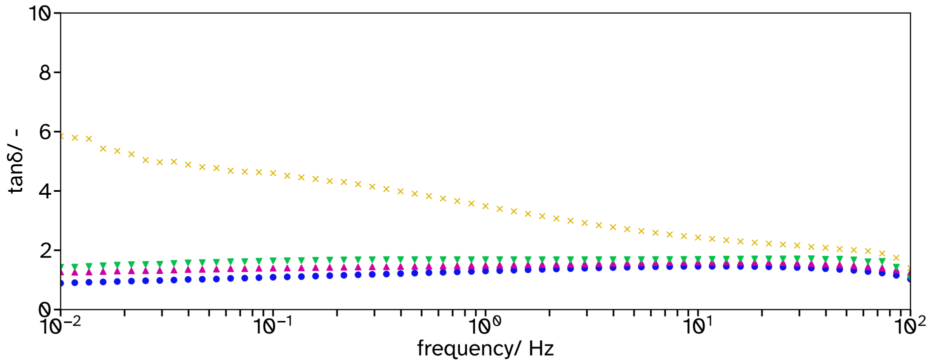

(c)

Figure S32: Rheological frequency sweeps of F_X13_Cn where n= 0.5 ●, 1 ▲, 2 ▼, and 4 ×.

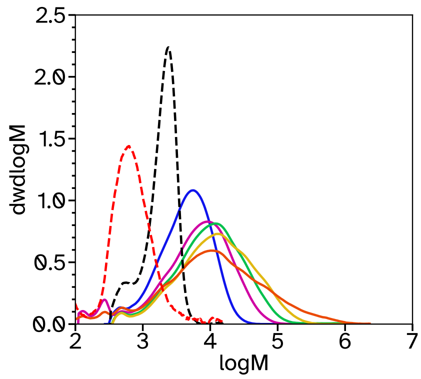

Figure S33: The final molecular weight distributions from conventional SEC analysis for F_Xn_C4, where n= 0 ■, 8 ■, 11 ■, 13 ■ and 18 ■ where the surfactant molecular weight distributions for Brij L23 (- - -) and Lakeland PAE 136 (- - -) are also shown.